Meyer CH (ed): Vital Dyes in Vitreoretinal Surgery.
Dev Ophthalmol. Basel, Karger, 2008, vol 42, pp 5–28

To See the Invisible: The Quest of Imaging Vitreous

J. Sebag

VMR Institute, University of Southern California, Los Angeles, Calif., USA

Abstract

Purpose: Imaging vitreous has long been a quest to view what is, by design, invisible. This chapter will review important historical aspects, past and present imaging methodologies, and new technologies that are currently in development for future research and clinical applications. **Methods:** Classic and modern histologic techniques, dark-field slit microscopy, clinical slit lamp biomicroscopy, standard and scanning laser ophthalmoscopy (SLO), ultrasonography, optical coherence tomography (OCT), combined OCT-SLO, magnetic resonance and Raman spectroscopies, and dynamic light scattering methodologies are presented. **Results:** The best available histologic techniques for imaging vitreous are those that avoid rapid dehydration of vitreous specimens. Dark-field slit microscopy enables in vitro imaging without dehydration or tissue fixatives. OCT enables better in vivo visualization of the vitreoretinal interface than SLO and ultrasonography, but does not adequately image the vitreous body. The combination of OCT with SLO has provided useful new imaging capabilities, but only at the vitreoretinal interface. Dynamic light scattering can evaluate the vitreous body by determining the average sizes of vitreous macromolecules in aging, disease, and as a means to assess the effects of pharmacologic vitreolysis. Raman spectroscopy can detect altered vitreous molecules, such as glycated collagen and other proteins in diabetic vitreopathy and possibly other diseases. **Conclusions:** A better understanding of normal vitreous physiology and structure and how these change in aging and disease is needed to develop more effective therapies and prevention. The quest to adequately image vitreous will likely only succeed through the combined use of more than one technique to provide better vitreous imaging for future research and clinical applications.

Historical Perspective

Clear by design (fig. 1), vitreous has fascinated men for years. Among the early theories of vitreous structure that were reviewed by Duke-Elder [1] is a description that vitreous is composed of 'loose and delicate filaments surrounded by fluid'. This is remarkably close to present-day concepts. During the 18th and 19th centuries, however, there were no less than four very different theories of vitreous structure. In 1741, Demours formulated the *alveolar theory*, claiming that there are alveoli of fluid

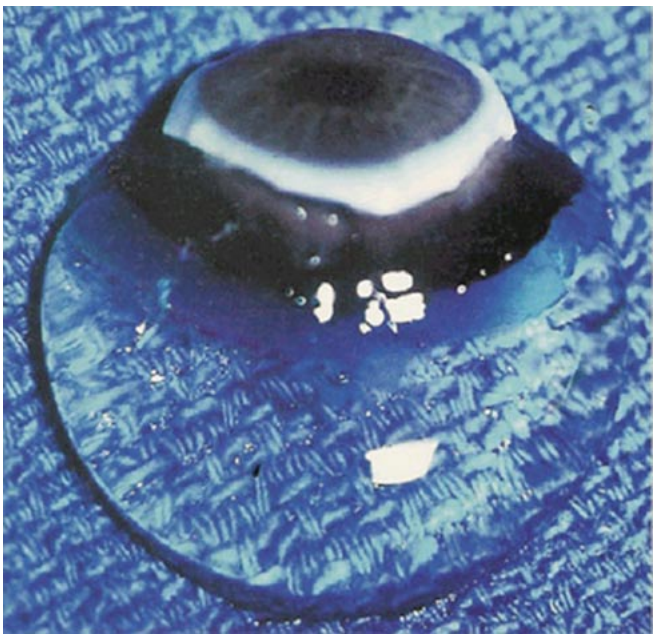

Fig. 1. Human vitreous body of a 9-month-old child dissected of the sclera, choroid, and retina, still attached to the anterior segment. Although the specimen is placed on a surgical towel in room air, the vitreous maintains its shape, because in youth the vitreous body is nearly entirely gel. Specimen courtesy of the New England Eye Bank.

between fibrillar structures. In 1780, Zinn proposed that vitreous is arranged in a concentric, lamellar configuration similar to the layers of an onion. The dissections and histologic preparations of Von Pappenheim and Brucke provided evidence for this *lamellar theory*. The *radial sector theory* was proposed by Hannover in 1845. Studying coronal sections at the equator, he described a multitude of sectors approximately radially oriented around the central anteroposterior core that contains Cloquet's canal. Hannover likened this structure to the appearance of a 'cut orange'. In 1848, Sir William Bowman established the *fibrillar theory*, which was based upon his finding microscopic fibrils, an observation which confirmed Retzius's earlier description of fibers that arose in the peripheral anterior vitreous and assumed an undulating pattern in the central vitreous, similar to a 'horse's tail'. In 1917, the elegant histologic preparations of Szent-Györgi supported these observations and introduced the concept that vitreous structure changes with age.

Unfortunately, the techniques employed in all these studies were flawed by artifacts that biased the results of the investigations. As pointed out by Baurmann and Redslob [2], these early histologic studies employed acid tissue fixatives that precipitated what we recognize today as the glycosaminoglycans hyaluronan (HA; formerly called hyaluronic acid), an effect which altered the histologic imaging of vitreous. Thus, the development of slit lamp biomicroscopy by Gullstrand in 1912 held great promise, as it was anticipated that this technique could enable imaging of vitreous structure without the introduction of fixation artifacts. Yet, as described by Redslob [2], a varied set of descriptions resulted over the years, ranging from a fibrous structure

to sheets, 'chain-linked fences', and various other interpretations. This problem even persisted in more recent investigations. Eisner [3] described 'membranelles', Worst [4] 'cisterns', Sebag and Balazs [5] 'fibers', and Kishi and Shimizu [6] 'pockets' in the vitreous. The observation of these so-called 'pockets' by the last-mentioned group was ultimately found to be an age-related phenomenon with little relevance to the normal macromolecular structure [7].

Vitreous Biochemistry

That vitreous is now considered an important ocular structure with respect to both normal physiology [8] as well as several important pathologic conditions of the posterior segment [9] is due in no small part to a better understanding of the biochemical composition and organization of vitreous. Vitreous biochemistry has been extensively reviewed elsewhere [10–12]. The features of vitreous biochemistry that are most relevant to this thesis concern the macromolecules HA and collagen, because these are the major constituents of vitreous along with water.

Hyaluronan

HA is a major macromolecule of vitreous. Although it is present throughout the body, HA was first isolated from bovine vitreous in 1934 by Meyer and Palmer. HA is a long, unbranched polymer of repeating disaccharide (glucuronic acid β-(1,3)-N-acetylglucosamine) moieties linked by β(1–4) bonds [13]. It is a linear, left-handed, threefold helix with a rise per disaccharide on the helix axis of 0.98 nm [14]. The sodium salt of HA has a molecular weight of $3–4.5 \times 10^6$ in normal human vitreous [15]. HA is not normally a free polymer in vivo, but is covalently linked to a protein core, the ensemble being called a proteoglycan.

Collagen

Recent studies [12] of pepsinized forms of collagen confirmed that vitreous contains collagen type II, a hybrid of types V/XI, and type IX collagen in a molar ratio of 75:10:15, respectively. In the entire body, only cartilage has as high a proportion of type II collagen as vitreous, explaining why certain inborn errors of type II collagen metabolism affect vitreous as well as joints. Vitreous collagens are organized into fibrils with type V/XI residing in the core, type II collagen surrounding the core, and type IX collagen on the surface of the fibril. The fibrils are 7–28 nm in diameter [16] but their length in situ is unknown.

Supramolecular Organization

As originally proposed by Balazs and more recently described with precision by Mayne [17], vitreous is a dilute meshwork of collagen fibrils interspersed with extensive arrays of HA molecules. The collagen fibrils provide a scaffold-like structure that is 'inflated' by the hydrophilic HA. If collagen is removed, the remaining HA forms a viscous solution; if HA is removed, the gel shrinks, but is not destroyed. On the basis of this and other observations, Comper and Laurent [18] proposed that electrostatic binding occurs between the negatively charged HA and the positively charged collagen in the vitreous.

Bishop [12] has proposed that to appreciate how vitreous gel is organized and stabilized requires an understanding of what prevents collagen fibrils from aggregating and by what means the collagen fibrils are connected to maintain a stable gel structure. Studies [12] have shown that the chondroitin sulfate chains of type IX collagen bridge between adjacent collagen fibrils in a ladder-like configuration spacing them apart. Such spacing is necessary for vitreous transparency, since keeping vitreous collagen fibrils separated by at least one wavelength of incident light minimizes light scattering, allowing the unhindered transmission of light to the retina for photoreception. Bishop [12] proposed that the leucine-rich repeat protein opticin is the predominant structural protein responsible for short-range spacing of collagen fibrils. Concerning long-range spacing, Scott et al. [19] and Mayne et al. [20] have claimed that HA plays a pivotal role in stabilizing the vitreous gel.

Several types of collagen-HA interactions may occur in different circumstances. Further investigation must be undertaken to identify the nature of collagen-HA interaction in vitreous. This question is important for an understanding of normal vitreous anatomy and physiology, but also as a means by which to understand the biochemical basis for age- and disease-related vitreous liquefaction and posterior vitreous detachment (PVD).

Vitreous Embryology

Interfaces

During invagination of the optic vesicle, the basal lamina of the surface ectoderm enters the invagination along with ectodermal cells that become specialized neural ectoderm. The cells lining the inner surface of the posterior wall of the optic vesicle (the posterior portion of the vesicle that does not invaginate) give rise to retinal pigment epithelium and its basal lamina, Bruch's membrane. The neural ectoderm that accompanies the invaginating anterior wall of the optic vesicle gives rise to the neural retinal cells and their underlying basal lamina, the internal limiting lamina (ILL). Thus, the basal laminae of both the retina and retinal pigment epithelium have the

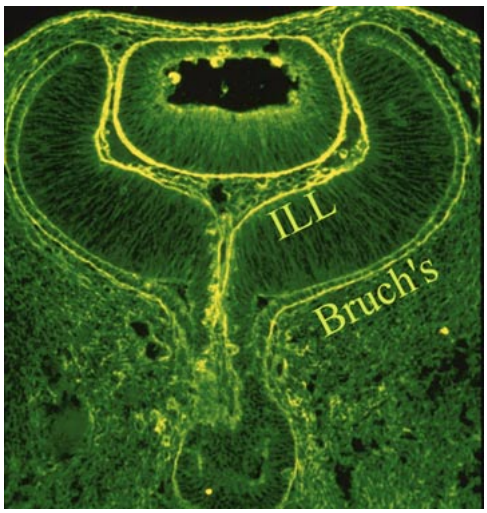

Fig. 2. Embryonic human eye. Posterior to the ILL is the neural retina. The tissue between the lens and the ILL will give rise to the vitreous. Anterior to Bruch's membrane is the retinal pigment epithelium. Of note is the fact that the ILL and Bruch's membrane are continuous, indeed the same structure. The indistinguishable origin of the ILL and Bruch's membrane is important in understanding neovascular (and perhaps other) pathologies of the vitreoretinal interface and the chorioretinal interface.

same embryologic origin. Figure 2 demonstrates the continuity of these two basal laminae. It is important to appreciate that these basal laminae serve as interfaces [21] between adjacent ocular structures. In the case of the ILL, this basal lamina is the interface between the retina and vitreous. Bruch's membrane separates the retinal pigment epithelium and retina from the choroid (neural crest origin).

These interfaces play an important role in a significant biological event that underlies one of the most devastating causes of blindness in humans, i.e. neovascularization. At the ILL interface between vitreous and retina, neovascularization in advanced diabetic retinopathy [22] and other ischemic retinopathies, including retinopathy of prematurity, is a significant cause of vision loss. At the level of Bruch's membrane, an interface of identical embryologic origin as the ILL, neovascularization in age-related macular degeneration is a significant and growing problem. Both of these conditions result from vascular endothelial cell migration and proliferation onto and into interfaces of the same embryologic origin – the basal lamina of the surface ectoderm. Improving our understanding of endothelial cell interaction with these interfaces should provide new insights into therapy and prevention of these important disorders.

Embryology of the Vitreous Body

Early in embryogenesis, the vitreous body is filled with blood vessels known as the vasa hyaloidea propia. This network of vessels arises from the hyaloid artery, which is directly connected to the central retinal artery at the optic disk. The vessels branch

many times within the vitreous body and anastomose anteriorly with a network of vessels surrounding the lens, the tunica vasculosa lentis. This embryonic vascular system attains its maximum prominence during the 9th week of gestation or 40-mm stage [23]. Atrophy of the vessels begins posteriorly with dropout of the vasa hyaloidea propria, followed by the tunica vasculosa lentis. At the 240-mm stage (7th month) in human beings, blood flow in the hyaloid artery ceases [24]. Regression of the vessel itself begins with glycogen and lipid deposition in the endothelial cells and pericytes of the hyaloid vessels [24]. Endothelial cell processes then fill the lumen and macrophages form a plug that occludes the vessel. The cells in the vessel wall then undergo necrosis and are phagocytized by mononuclear phagocytes [25]. Gloor [26], however, claimed that macrophages are not involved in vessel regression within the embryonic vitreous but that autolytic vacuoles form in the cells of the vessel walls, perhaps in response to hyperoxia. Interestingly, the sequence of cell disappearance from the primary vitreous begins with endothelial and smooth muscle cells of the vessel walls, followed by adventitial fibroblasts and lastly phagocytes [27], consistent with a gradient of decreasing oxygen tension.

It is not known precisely what stimulates regression of the hyaloid vascular system, but studies have identified a protein native to the vitreous that inhibits angiogenesis in various experimental models [28–31]. Teleologically, such activity seems necessary if a transparent tissue is to inhibit cell migration and proliferation and minimize light scattering to maintain transparency. This may also be the mechanism that induces regression of the vasa hyaloidea propia. Thus, activation of this protein and its effect on the primary vitreous may be responsible for the regression of the embryonic hyaloid vascular system as well as the inhibition of pathologic neovascularization in the adult. Hyaloid vessel regression may also result from a shift in the balance between growth factors promoting new vessels, such as vascular endothelial growth factor A, and those inducing regression, such as placental growth factor.

Recent studies [32, 33] have suggested that the vasa hyaloidea propria and tunica vasculosa lentis regress via apoptosis. Mitchell et al. [32] pointed out that the first event in hyaloid vasculature regression is endothelial cell apoptosis and proposed that lens development separates the fetal vasculature from vascular endothelial growth factor-producing cells, decreasing the levels of this survival factor for vascular endothelium, inducing apoptosis. Following endothelial cell apoptosis, there is loss of capillary integrity, leakage of erythrocytes into the vitreous, and phagocytosis of apoptotic endothelium by macrophages, which were felt to be important in this process. Subsequent studies by a different group [34] confirmed the importance of macrophages in promoting regression of the fetal vitreous vasculature and further characterized these macrophages as hyalocytes. Meeson et al. [35] proposed that there are actually two forms of apoptosis that are important in regression of the fetal vitreous vasculature. The first ('initiating apoptosis') results from macrophage induction of apoptosis in a single endothelial cell of an otherwise healthy capillary segment with normal blood flow. The isolated dying endothelial cells project into the capillary

lumen and interfere with blood flow. This stimulates synchronous apoptosis of downstream endothelial cells ('secondary apoptosis') and ultimately obliteration of the vasculature. Removal of the apoptotic vessels is achieved by hyalocytes.

A better understanding of this phenomenon may provide insights into new ways to induce the regression of pathologic angiogenesis or inhibit neovascularization in such conditions as proliferative diabetic retinopathy and exudative age-related macular degeneration. Indeed, the recently developed synthetic vascular endothelial growth factor inhibitors seem to be of limited usefulness in treating pathologic neovascularization in exudative age-related macular degeneration. However, this or a superior inhibitory mechanism may prove to be useful in other proliferative retinopathies, such as retinopathy of prematurity.

Vitreous Imaging

Previously considered a vestigial organ, vitreous is now regarded as an important ocular structure [8, 9], at least with respect to several important pathologic conditions of the posterior segment. This remarkable tissue is in essence an extended extracellular matrix, composed largely of water with a very small amount of structural macromolecules [9, 10]. Nevertheless, in the normal state it is a solid and clear gel, especially in youth (fig. 1). Because of the predominance of water within vitreous, effective imaging of this structure in vitro is best performed by methods that overcome the intended transparency of this tissue yet avoid dehydration. Imaging vitreous in vivo is likely best achieved by visualizing the macroscopic features via an assessment of the nature and organization of the molecular components. The following will review some of the most important methods available for imaging vitreous in vitro and in vivo.

In vitro Imaging

Arguably the best available technique for the histologic characterization of vitreous structure was developed by Faulborn. Through an arduous process of tissue preparation that very slowly dehydrates specimens over months, this technique minimizes the disruption of vitreous structure that results from the rapid dehydration that is induced by standard histologic tissue processing. The elegant preparations obtained with such slow dehydration have provided great insight into the role of vitreous in the pathophysiology of proliferative diabetic vitreoretinopathy [22] (fig. 3) and retinal tears [36] (fig. 4).

Dark-field slit microscopy of whole human vitreous in the fresh, unfixed state was extensively employed by Sebag and Balazs [37] to characterize the fibrous structure of vitreous (fig. 5), age-related changes within the central vitreous body [38] and at the

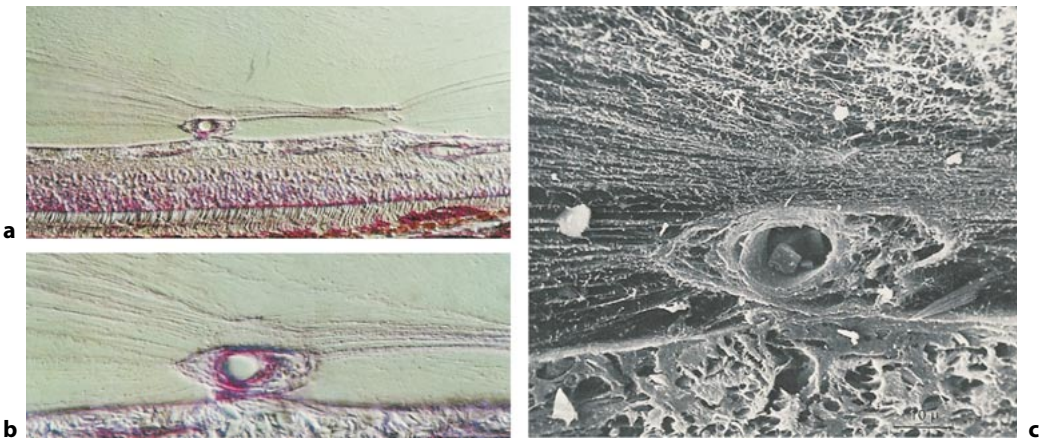

Fig. 3. Proliferative diabetic vitreoretinopathy. Neovascularization which arises from the disk and retina involves vascular endothelial cell migration and proliferation onto and into the posterior vitreous cortex. These photomicrographs demonstrate the formation of neovascular complexes sprouting into the posterior vitreous cortex of a human eye (bar = 10 μm). Reprinted with permission from Faulborn and Bowald [22].

vitreoretinal interface [39], and the effects of diabetes on human vitreous structure [40]. This imaging method has clearly demonstrated the fibers in the anterior peripheral vitreous (fig. 6) that transmit traction to the peripheral retina in rhegmatogenous retinal pathology. Fibers in this region also play a role in the formation of the so-called 'anterior loop' configuration of anterior proliferative vitreoretinopathy (fig. 7). Traction mediated by this anterior loop causes ciliary body detachment (sometimes with hypotony) and iris retraction in severe cases.

In vivo Imaging

Conventional Ophthalmoscopy and Biomicroscopy

Of all the parts of the eye that are routinely evaluated by physical examination, vitreous is perhaps the least amenable to standard inspection techniques. This is because examining vitreous is an attempt to visualize a structure designed to be virtually invisible [42]. With the direct ophthalmoscope light rays emanating from a point in the patient's fundus emerge as a parallel beam which is focused on the observer's retina and an image is formed. However, incident light reaches only the part of the fundus onto which the image of the light source falls and only light from the fundus area onto which the observer's pupil is imaged reaches that pupil. Thus, the fundus can be seen only where the observed and the illuminated areas overlap and where the light source and the observer's pupil are aligned optically. This restricts the extent of

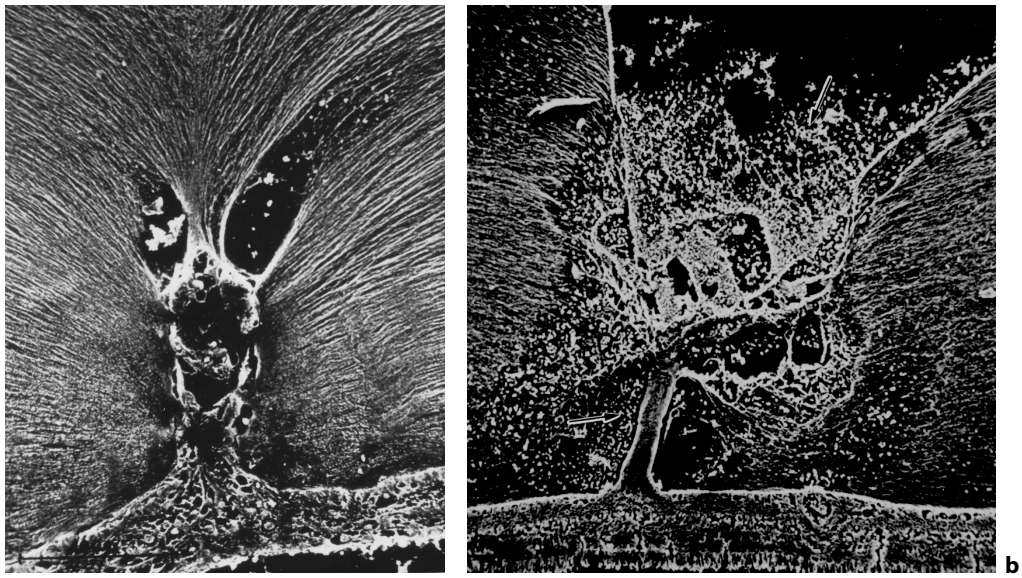

Fig. 4. Morphology of peripheral vitreous. **a** Cystic retinal tuft. The tuft is a cystoid formation of fibers, similar to those of the nerve fiber layer, and cells, similar to those found in the inner plexiform layer of the retina. The tuft is connected to the ILL of the retina. This scanning electron micrograph shows the insertion of the vitreous collagen fibers on the tuft's apical surface. Their orientation changes toward the tuft's surface. Reprinted with permission from Dunker et al. [36]. **b** Verruca. The verruca has a structure similar to that of a tree. Its 'roots' are embedded in the inner layers of the retina. Cellular elements resembling cells of the inner plexiform layer can be seen near the retinal surface. The 'trunk' of this structure extends from the retina to the middle parts of the vitreous cortex. The 'branches' of the verruca are intertwined with interrupted vitreous collagen fibers. Local condensation of collagen fibers exists as well as local collagen destruction (arrows) and interruption of the ILL of the retina. Reprinted with permission Dunker et al. [36].

the examined area and also because of a limited depth of field, this method is rarely used to assess vitreous structure.

Indirect ophthalmoscopy was one of the major contributions of Charles Schepens to the world. It extends the field of view by using an intermediate lens to gather rays of light from a wider area of the fundus. While this technique has been invaluable in the diagnosis and treatment of various vitreoretinal disorders, its use in vitreous alone has been more limited. This is due to the fact that although binocularity provides stereopsis, the image size is considerably smaller than with direct ophthalmoscopy and only significant alterations in vitreous structure, such as a hole in the prepapillary posterior vitreous cortex, vitreous hemorrhage, or asteroid hyalosis, are reliably diagnosed by indirect ophthalmoscopy. The most difficult clinical entity to assess is that of PVD, particularly when anomalous.

Effectively using slit lamp biomicroscopy to overcome vitreous transparency necessitates maximizing the Tyndall effect. Although this can be achieved in vitro, as

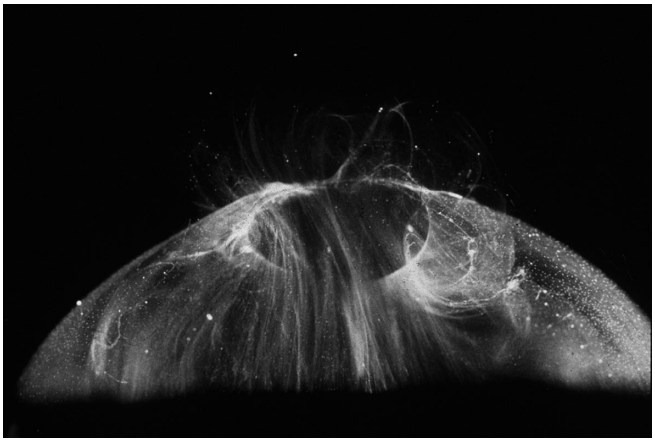

Fig. 5. Posterior and central vitreous of a 59-year-old man. The premacular hole is to the top at the center. Fibers course anteroposteriorly in the center of the vitreous and enter the retrocortical (preretinal) space via the premacular region of the vitreous cortex. Within the cortex are many small 'dots' that scatter light intensely. The larger, irregular dots are debris. The small dots are hyalocytes.

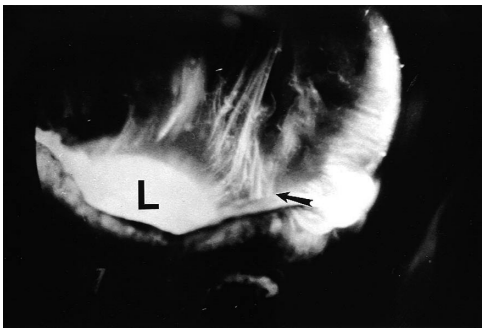

Fig. 6. Vitreous base morphology. Vitreous structure in a 58-year-old female. Fibers course anteroposteriorly in the central and peripheral vitreous. Posteriorly, fibers orient to the premacular region. Anteriorly, the fibers 'splay out' to enter into the vitreous base (arrow). L = Crystalline lens.

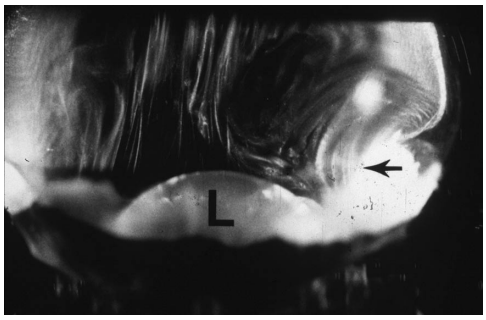

Fig. 7. Vitreous base 'anterior loop'. Central and peripheral vitreous structure in a 76-year-old male. The posterior aspect of the lens is seen below. Fibers course anteroposteriorly in the central vitreous and enter at the vitreous base. The 'anterior loop' configuration at the vitreous base is seen on the right side of the specimen. L = Lens; arrow = anterior loop of vitreous base. Reprinted with permission from Sebag and Balazs EA [41].

described above, there are limitations to the illumination/observation angle that can be achieved clinically. This is even more troublesome in the presence of meiosis, corneal and/or lenticular opacities, and limited patient cooperation. Essential to the success of achieving an adequate Tyndall effect are maximizing pupil dilation in the

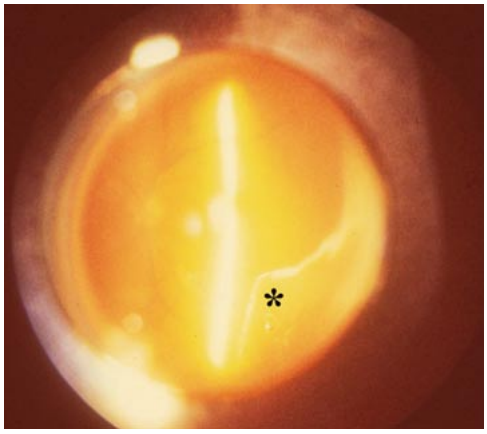

Fig. 8. Fundus photograph of PVD. The detached posterior vitreous cortex (asterisk) can be seen anterior to the optic disk (to the left). Courtesy of Clement Trempe, MD.

patient, since the Tyndall effect increases with an increasingly subtended angle between the plane of illumination and the line of observation (up to a maximum of 90°), and dark adaptation in the examiner. Some observers purport that green light enhances the Tyndall effect, although this has never been explained or tested scientifically. Preset lens biomicroscopy attempts to increase the available illumination-observation angle, offers dynamic inspection of vitreous in vivo, and provides the capability of recording the findings in real time [43]. Initially introduced on a wide scale for use with a Hruby lens and currently practiced by using a hand-held 90-diopter lens at the slit lamp, this technique is purportedly best performed with a fundus camera and the El Bayadi-Kajiura lens promoted by Schepens et al. [43] (fig. 8). This approach has been used in many seminal studies of the role of vitreous in various disease states. However, there has not been widespread use of this approach, probably because it is heavily dependent upon subjective interpretation of the findings and questionable reproducibility from center to center.

Scanning Laser Ophthalmoscopy

The scanning laser ophthalmoscope was developed at the Schepens Eye Research Institute in Boston to enable dynamic inspection of vitreous in vivo. Scanning laser ophthalmoscopy (SLO) features tremendous depth of field, and offers real-time recording of findings. Monochromatic green, as well as other wavelengths of light are also available for illumination [44]. SLO has improved our ability to visualize details in the prepapillary posterior vitreous, such as Weiss's ring. Unfortunately, in spite of the dramatic depth of field possible with this technique, SLO does not adequately image the entire vitreous body and, in particular, the attached posterior vitreous cortex, probably because its thickness is below the SLO level of resolution. Thus, PVD, by far the most common diagnosis to be entertained when imaging vitreous clinically, is

not reliably identified by SLO. Indeed, there is an increasing awareness among vitreous surgeons that the reliability of the clinical diagnosis of total PVD by any existing technique is woefully inadequate. This awareness arises from the fact that vitreous surgery following clinical examination often reveals findings that are contradictory to preoperative assessments.

Ultrasonography

Ultrasound is an inaudible acoustic wave that has a frequency of more than 20 kHz. The frequencies used in ophthalmology are generally in the range of 8–10 MHz. Although these very high frequencies produce wavelengths as short as 0.2 mm, these are not short enough to adequately assess normal internal vitreous structure such as the fibers described above. Even the posterior vitreous cortex, about 100 μm at its thickest point in the normal state, is below the level of resolution of conventional ultrasonography. The utility of this technique results from the fact that strong echoes are produced at 'acoustic' interfaces found at the junctions of media with different densities and sound velocities, and the greater the difference in density between the two media that create the acoustic interface, the more prominent the echo. Thus, age-related or pathologic phase alterations within the vitreous body are detectable by ultrasonography.

In the late 1950s and early 1960s, Oksala was among the first to employ B-scan ultrasonography to image vitreous. The findings of his extensive study of aging changes were summarized in 1978 [45]. In that report of 444 'normal' subjects, Oksala defined the presence of acoustic interfaces within the vitreous body as evidence of vitreous aging and determined that the incidence of such interfaces was 5% between the ages of 21–40 years, and fully 80% in individuals over 60 years of age. In clinical practice, however, only profound entities such as asteroid hyalosis, vitreous hemorrhage, and intravitreal foreign bodies (if sufficiently large) are imaged by ultrasonography.

At the vitreoretinal interface, the presence of a PVD is often suspected on the basis of B-scan ultrasonography but can never be definitively established, since the level of resolution of ultrasound is not sufficient to reliably image the posterior vitreous cortex, which is only a little more than 100 μm at its thickest portion. In essence, while the presence of PVD can often be reliably established by ultrasound, its absence cannot. Clinical studies [46] have successfully used this technique to determine that in patients with proliferative diabetic vitreoretinopathy [47], there is a split in the posterior vitreous cortex, called vitreoschisis (fig. 9). The success achieved in using ultrasound to identify this important pathologic entity probably results from the fact that this tissue is abnormally thickened by nonenzymatic glycation of vitreous collagen and other proteins [49]. When not thickened, and indeed when vitreoschisis in nondiabetic patients causes the posterior vitreous cortex to be thinner than normal, the thickness of these tissue planes falls below the level of resolution of this imaging modality.

Fig. 9. Ultrasonography imaging of vitreoschisis. Splitting of the vitreous cortex (arrow) can occur and mimic PVD. In diabetic patients, blood can be present in the vitreoschisis cavity. When the blood cells settle to the bottom of the vitreoschisis cavity, a 'boat-shaped' preretinal hemorrhage can result. I = Inner wall; P = posterior wall of the vitreoschisis cavity within the posterior vitreous cortex. Photograph courtesy of Dr. Ronald Green. Reprinted with permission from Green and Byrne [48].

Optical Coherence Tomography

Invented by Fujimoto at MIT and introduced into clinical practice in 1991, optical coherence tomography (OCT) is a new technique for cross-sectional imaging of ocular structures [50]. OCT is based on the principle of low-coherence interferometry, where the distances between and sizes of structures in the eye are determined by measuring the time it takes for light to backscatter from structures at varied axial distances. The resolution of all 'echo'-based imaging technologies (such as ultrasound and OCT) is based upon the ratio of the speed of the incident wave to that of the reflected wave. As described above, vitreoretinal ultrasonography is usually performed with a frequency of 10 MegaHz and has a 150-mm resolution. Although recently introduced ultrasound biomicroscopy has increased the frequency (up to 100 MegaHz), and thus has a spatial resolution of 20 μm, penetration into the eye is no more than 4–5 mm. Light-based devices, such as the OCT, use an incident wavelength of 800 nm and have increased axial resolution to 10 μm, providing excellent imaging of retinal architecture. The limitations of OCT include the inability to obtain high-quality images through media opacities such as dense cataract or vitreous hemorrhage. Furthermore, much of the vitreous body is not presently imaged by OCT, limiting the utility of this technique for vitreous imaging.

To date, OCT has primarily been used to image, and to some extent quantitate, structure and pathologies in the retina, subretinal space, retinal pigment epithelium, and choroid. Vitreous applications that have been useful involve imaging the vitreomacular interface in patients with macular pucker, vitreomacular traction syndrome, diabetic macular edema, and macular holes [51]. Often, however, the exact nature and molecular composition of these preretinal tissue planes cannot be definitively deduced using conventional time domain OCT.

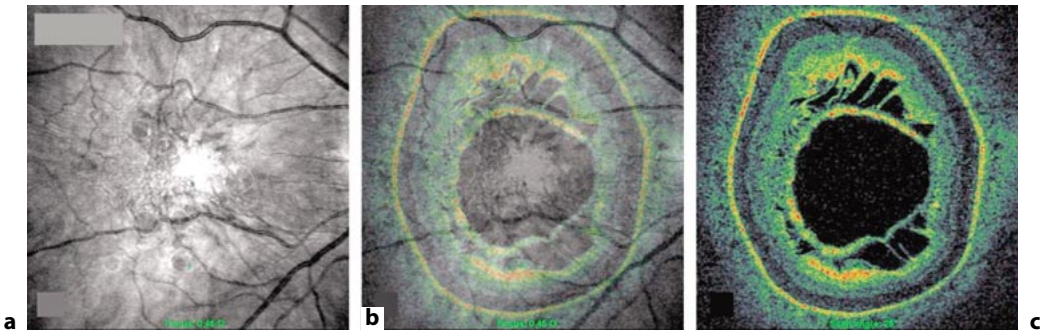

Fig. 10. Coronal plane imaging with combined OCT-SLO. The SLO grayscale fundus image (**a**) overlaid upon the coronal OCT color image (**c**) results in a superimposed image (**b**) used to identify the number of retinal contraction centers in macular pucker.

Combined OCT-SLO

Combined OCT-SLO imaging (OPKO, Inc., Toronto, Canada) is a new imaging technology that consists of a dual channel system incorporating an interferometer and a confocal receiver. A broadband infrared superluminescent diode with a wavelength of 820 nm provides the light source. In the longitudinal mode, the OCT-SLO projects light through a Galvano scanning mirror system, moving the beam in a horizontal line to create cross-sectional images of the retina. In the coronal imaging mode (created by transverse scanning), the light is projected through 2 x-/y-plane Galvano scanners moving the beam in a raster fashion across the surface of the retina. Each coronal plane image that is produced is an x-/y-image at a different z-axis depth. The depth resolution is approximately 10 μm while the transverse resolution is approximately 20 μm. For both the coronal and longitudinal OCT scans, a matching grayscale confocal fundus image is also produced. The grayscale SLO confocal fundus image (fig. 10a) and the threshold color OCT image in the coronal plane (fig. 10c) can be superimposed (fig. 10b). There is pixel-to-pixel registration between the two images (coronal OCT and SLO) since they are obtained simultaneously using parallel detector systems. The superimposed coronal plane images are especially useful for identifying centers of retinal contraction in macular pucker, defined as an area where radially oriented retinal striations converge. This feature has also been used to identify the presence of retinal contraction in patients with macular holes.

Coronal plane OCT-SLO imaging studies [52] in 44 patients with macular pucker found multiple foci of retinal contraction and pucker in 20 of the 44 patients (45.5%). Table 1 demonstrates the distribution of the number of pucker centers as identified by SLO-OCT imaging in the coronal plane.

Two distinct foci of retinal contraction (fig. 11b) were detected in 11/44 patients (25%), 3 different sites (fig. 11c) were identified in 5/44 patients (11.4%), and 4/44 (9.1%) had 4 centers of retinal contraction (fig. 11d). Intraretinal cysts were present

Table 1. Stratification of pucker centers demonstrates that nearly half of all membranes (20/44 = 45.5%) have more than one retinal contraction center

Number of retinal contraction centers	One	Two	Three	Four
Number of patients	24	11	5	4
Patient population, %	54.5	25.0	11.4	9.1

in 10/35 (28.6%) subjects with 1 or 2 pucker centers as compared to 6/9 (66.7%) subjects with 3 or 4 centers ($p = 0.05$, Fisher's exact test). The average macular thickness of subjects with 1 or 2 pucker centers was 297 ± 110 versus $369 \pm 98\,\mu m$ for subjects with 3 or 4 pucker centers ($p = 0.05$, t test assuming equal variance). Thus, coronal plane imaging with combined OCT-SLO technology revealed multifocality in macular pucker that has clinical significance. Since eyes with multiple retinal contraction centers had intraretinal cysts twice as frequently, and greater retinal thickening as compared to eyes with only 1 or 2 contraction centers, this may not only impact upon prognosis, but management as well, in that eyes with multiple contraction centers may need to undergo surgery sooner than unifocal cases.

Combined OCT-SLO also enables visualization of the intersecting planes of fundus imaging by SLO in the x-/y-plane, and by OCT in the z-plane (fig. 12). This manufacturer-provided 3-dimensional rendering of the intersection between a longitudinal OCT scan and the SLO image can be used to identify a variety of abnormalities, particularly those that are difficult to visualize, such as vitreopapillary traction, or the centers of an area of retinal contraction in multifocal macular pucker. The SLO fundus images with superimposed coronal plane OCT scans can be analyzed quantitatively with Adobe PhotoShop software, an approach that has proven very useful for quantitative analysis of vitreoretinal topography in macular pucker [55].

In a study [56] of 25 patients with macular holes, OCT-SLO found eccentric macular pucker in 40% of cases. This would have been difficult, if not impossible, to reliably visualize with conventional OCT. Further analysis [57] revealed that when compared to eyes with unifocal macular pucker and no macular holes, the eccentric pucker in patients with macular holes had an average surface area of contraction of $23.12 \pm 18.8\,mm^2$ that was significantly smaller than in macular pucker eyes ($63.2 \pm 23.7\,mm^2$; $p = 0.006$). Also, the distance from the center of retinal contraction to the center of the macula was significantly greater in macular hole eyes ($8.64 \pm 2.33\,mm$) than macular pucker eyes ($4.45 \pm 1.9\,mm$; $p = 0.0001$).

High-resolution time domain OCT-SLO and the newer spectral domain imaging technologies have provided even more powerful methods with which to evaluate the vitreoretinal interface. As a result, new concepts of disease pathogenesis are evolving. For example, vitreoschisis, defined as a split in the posterior vitreous cortex, has pre-

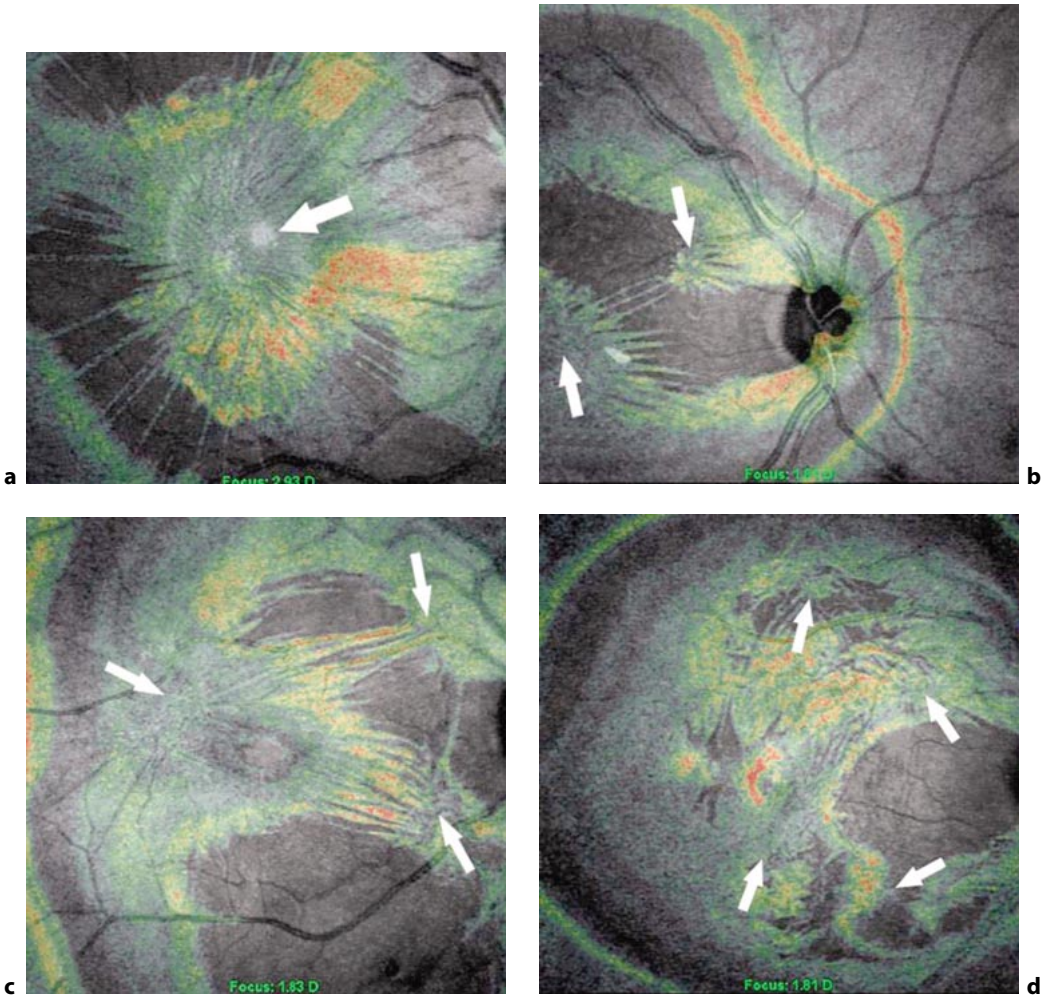

Fig. 11. Coronal plane imaging of macular pucker with combined OCT-SLO. Superimposing coronal plane OCT color images upon the SLO grayscale fundus image reveals multifocality (arrows) in the topography of macular pucker. **a** 1 pucker (retinal contraction) center. **b** 2 centers. **c** 3 centers. **d** 4 centers.

viously been described in proliferative diabetic vitreoretinopathy [47] by ultrasound [46]. However, high-resolution time domain OCT-SLO can better detect this condition in proliferative diabetic vitreoretinopathy than ultrasound (fig. 13). Moreover, studies [57] with high-resolution time domain OCT-SLO have detected vitreoschisis in 24/45 eyes (53.3%) with macular holes, and in 19/44 (43.2%) with macular pucker. Anomalous PVD may be the inciting event in each of these conditions [58]. However, as mentioned above, the topographic and structural features that were detected in eyes with macular holes and eccentric retinal contraction differed in comparison to eyes with macular pucker alone [57], suggesting that while each condition may begin

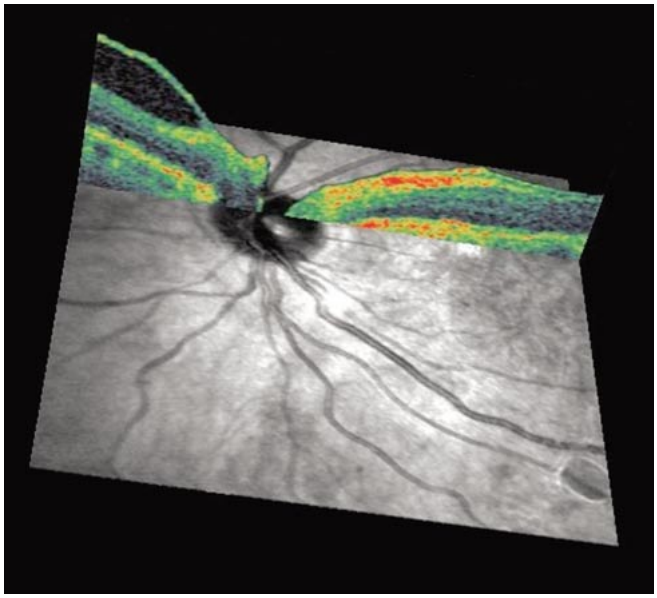

Fig. 12. Three-dimensional OCT-SLO Imaging of vitreopapillary traction. The color OCT image can be intersected with the grayscale SLO fundus image to detect exactly where on the fundus an OCT finding is located. In this eye there is obvious insertion of a vitreous membrane onto the optic disk. In some cases, this can induce optic nerve dysfunction [53]. Vitrectomy can eliminate this form of anomalous PVD [58], with improvements in visual function [54].

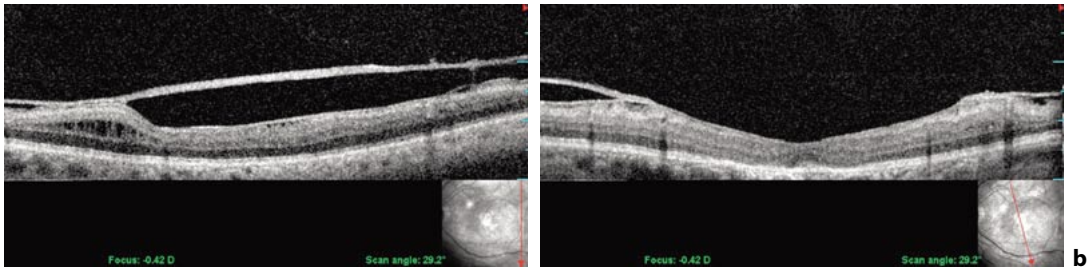

Fig. 13. OCT-SLO imaging of vitreoschisis in proliferative diabetic vitreoretinopathy. A split in the posterior vitreous cortex is visible (arrowhead) on combined OCT-SLO transverse imaging. Significant retinal traction is induced at the point where the two layers of the split posterior vitreous cortex rejoin to form a full-thickness cortex. Often, this is the site of traction retinal detachment.

with anomalous PVD, differences in subsequent cell migration and proliferation probably result in the different clinical appearances. The considerable detail that is afforded by spectral domain imaging will very likely shed more light upon this and other questions.

It is important to note, however, that in spite of the high resolution provided by these imaging technologies, they are still only evaluating changes at the tissue level [59]. Much earlier in the natural history of the disease there are molecular and physiological

changes that eventually result in the subsequent cellular and tissue changes. If we are ever to develop preventative therapies, future diagnostic technologies will need to de obtained that can assess ocular health and deviations from this state of health on a molecular and physiologic level. The following presents some of the approaches that are currently in development.

Spectroscopy

Nuclear Magnetic Resonance Spectroscopy. The nuclear magnetic resonance (NMR) spectroscopy phenomenon is based upon the fact that when placed in a magnetic field, nuclei (especially water protons) orient their magnetic vectors along the direction of the magnetic field. The time constant for this orientation, known as the longitudinal relaxation time T_1, reflects the thermal interactions of protons with their molecular environment. Magnetic vectors that have previously been induced to be in phase with each other undergo a 'dephasing' relaxation process that is measured by the transverse relaxation time T_2. It is the transverse relaxation time T_2 that reflects inhomogeneities within the population of protons. Protons oriented by a magnetic field absorb radio waves of the appropriate frequency to induce transactions between their two orientations. Such absorption is the basis of the NMR signal used to index relaxation times. Relaxation times in biologic tissues vary with the concentration and mobility of water within the tissue. As the latter is influenced by the interaction of water molecules with macromolecules in the tissue, this noninvasive measure can assess the gel-to-liquid transformation that occurs in vitreous during aging [38] and disease states, such as diabetic vitreopathy [47, 60]. These considerations led Aguayo et al. [61] to use NMR spectroscopy in studying the effects of pharmacologic vitreolysis [62] of bovine and human vitreous specimens and intact bovine eyes in vitro. Collagenase induced measurable vitreous liquefaction more than hyaluronidase. Thus, this noninvasive method could be used to evaluate age- and disease-induced synchisis (liquefaction) of the vitreous body, although it is not clear whether this technique adequately evaluates the vitreoretinal interface. More recently, NMR spectroscopy has been employed in studies of retinal structure [63] or the measurement of vitreous oxygen as an index of retinal oxygen metabolism [64, 65]. Pilot clinical studies [66] have also attempted to use this technology to index a diabetes-induced breakdown of the blood-retinal barrier. Curiously, few recent studies have investigated intrinsic vitreous structure using this imaging technology.

Raman Spectroscopy. This form of spectroscopy was first described in 1928 by C.V. Raman in India. Raman spectroscopy is an inelastic light scattering technique wherein the vibrational-mode molecules in the study specimen absorb energy from incident photons, causing a downward frequency shift, which is called the Raman shift. Because the signal is relatively weak, current techniques employ laser-induced stimulation with gradual increases in the wavelength of the stimulating laser, so as to be able to detect the points at which the Raman signal becomes apparent as peaks superimposed on the

broad background fluorescence. The wavelengths at which these peaks are elicited are characteristic of the chemical bonds, such as aliphatic C—H (2,939 cm^{-1}), water O—H (3,350 cm^{-1}), C═C and C—H stretching vibrations in π-conjugated and aromatic molecules (1,604 cm^{-1} and 3,057 cm^{-1}). To date, most applications of this technique in the eye have been for analysis of lens structure and pathology [67]. The use of near-infrared excitation wavelengths is particularly effective in the lens, since these wavelengths have better penetration into opacified lenses with cataracts.

The first vitreous Raman spectroscopy studies [68] employed excised human vitrectomy samples obtained during surgery. The near-infrared excitation at 1,064 nm was provided by a diode-pumped Nd:YAG CW laser with a diameter of 0.1 mm and a power setting of 300 mW. Backscattering geometry with an optical lens collected scattered light which was passed through a Rayleigh light rejection filter into a spectrophotometer. The results showed that this technique was able to detect peaks at 1,604 cm^{-1} and 3,057 cm^{-1} in vitreous of diabetic patients that were not present in controls. Further research and development is needed to refine the methodology for use in situ, and eventually in vivo, with the ultimate aim of providing a noninvasive technique to assess the tissue effects of diabetes as an adjunct to monitoring blood glucose levels. Not only would this provide another evaluation of diabetes effects on the eye, but might also enable the use of the eye as a window to the body, since these phenomena are ubiquitous.

Recent studies have used Raman spectroscopy to detect the presence of β-carotene in vitreous that was removed at surgery for asteroid hyalosis [69]. Another application of Raman spectroscopy has been to detect intravitreal glutamate levels in vitro [70]. While this approach does not provide information about vitreous anatomy and physiology, it does have potential as a noninvasive way to evaluate intraocular physiology in diabetic retinopathy and glaucoma.

Dynamic Light Scattering

Dynamic light scattering (DLS) is an established laboratory technique to measure the average size (or size distribution) of microscopic particles as small as 3 nm in diameter that are suspended in a fluid medium where they undergo random brownian motion. Light scattered by a laser beam passing through such a dispersion will have intensity fluctuations in proportion to the brownian motion of the particles, resulting in a constantly fluctuating speckle pattern [71]. This speckle pattern is the result of interference in the light paths and it fluctuates as the particles in the scattering medium undergo random movements on a time scale of $\geq$1 μs due to the collisions between themselves and the fluid molecules (brownian motion). Since the size of the particles influences their brownian motion, analysis of the scattered light intensity yields a distribution of the size(s) of the suspended particles. In dilute dispersions, generally the case in biologic tissues, especially in the eye, light scattered from small particles fluctuates rapidly while light scattered from large particles fluctuates more slowly. Calibration and comparison to standards enables the determination of actual

particle sizes. In circumstances where there is an active increase (or decrease) in particle sizes (from nanometers to a few micrometers) and/or an increase (or decrease) in the number or density of suspended particles, the result is an increase in scattered light intensity, or polydispersity, which is a measure of the number of distinct groups of species with different sizes. Thus, a change in scattered light intensity and polydispersity can complement particle size determination.

In the eye, visible light from a laser diode (670 nm, power = 50 μW) is focused into the tissue of interest, and backscattered light is collected for analysis. The detected signal is processed via a digital correlator to yield a time autocorrelation function. For dilute dispersions of spherical particles the slope of the time autocorrelation function provides a quick and accurate determination of the particle's translational diffusion coefficient, which can be related to its size via a Stokes-Einstein equation, provided the viscosity of the suspending fluid, its temperature, and its refractive index are known. For the lens and vitreous, a viscosity of $\eta = 0.8904$ cP, a refractive index of $n = 1.333$, and a temperature of 25°C for in vitro studies and 37°C for in vivo studies were used to determine macromolecule sizes.

Ansari [72] has recently authored an overview of ophthalmic applications of DLS and their current state of development. Most of the work has been done in the lens [73], where studies found that DLS was able to detect and quantify the changes induced in a hyperbaric oxygen model of nuclear cataract [74]. In fact, DLS was more sensitive than Scheimpflug photography in detecting early changes in a cold cataract model [75]. A large cross-sectional clinical study performed at the National Eye Institute has been conducted and the results have been submitted for publication.

DLS of vitreous provides information such as diffusion coefficient, particle size, scattered intensity, and polydispersity (measure of heterogeneity). Early studies determined that with this DLS apparatus bovine [76] and human [77] vitreous exhibit bimodal behavior, consistent with the two-component composition of vitreous (HA and collagen macromolecules). In diabetes, there are considerable changes in vitreous biochemistry [49] that induce structural changes [40] due to the aggregation of vitreous proteins, particularly collagen. DLS was not only able to detect, but also quantify these changes on a molecular level [77]. Thus, with this advanced imaging technology, it might be possible to characterize the molecular effects of diabetes on the eye and indeed use the eye as an index for diabetes effects on the entire body. Detecting and characterizing the molecular effects of diabetes in this noninvasive manner will deepen our understanding of the pathophysiology and enable treatments at a very early stage of disease. Repeat testing can be performed often so as to monitor the response to therapy. Such intervention will likely prevent disease advancement to cellular and tissue levels, and ultimately prevent organ failure.

Pharmacologic vitreolysis [62, 78] is a new approach to vitreoretinal therapeutics. The objective is to alter vitreous biochemistry with the intent of eliminating the contribution of vitreous to retinal disease. Since an innocuous (PVD depends upon

both liquefaction of the gel and dehiscence at the vitreoretinal interface, agents are being developed to achieve both of these objectives. Substances that liquefy the gel are called 'liquefactants', while those that alter the vitreoretinal interface are known as 'interfactants' [11]. Since agents such as hyaluronidase (Vitrase®) and perhaps plasmim/microplasmin are predominantly liquefactants, their effects must be monitored closely to prevent untoward effects. This is needed to avoid the inadvertent induction of anomalous PVD [58] that might result from inducing excess or precocious liquefaction before adequate vitreoretinal dehiscence has been created. Thus, noninvasive, reproducible, and rapid diagnostic systems need to be developed that can monitor the process of pharmacologic vitreolysis.

Advancement of the field of pharmacologic vitreolysis would greatly benefit from the development of diagnostic technologies that can enable molecular assessment of the state of the vitreous and changes therein. Studies have shown that DLS can provide useful information regarding various aspects of vitreous biochemistry. This molecular diagnostic methodology was shown to be effective in detecting and quantifying the changes induced by hyaluronidase, collagenase, and microplasmin [79]. Indeed, the use of DLS in studying microplasmin showed that this technique could be very useful in quantifying effects on vitreous diffusion coefficients [80], an important property for both health and disease of the vitreous.

Conclusions

The development of new treatments for the cure or prevention of vitreoretinal diseases requires new insights into the causes and progression of these disorders [81]. No single method presently exists that will enable accurate and reproducible noninvasive imaging of both the vitreous body and the vitreoretinal interface. This impacts significantly upon the ability to assess the effects of aging and disease and, in particular, upon the accuracy of diagnosing posterior vitreous detachment clinically. Moreover, this limitation hinders our ability to adequately evaluate the role of vitreous in vitreoretinal diseases such as retinal detachment, both in general terms and in specific clinical cases.

Today, combining more than one of the aforementioned techniques could provide considerably more information than just one technique. For example, NMR spectroscopy could assess the degree of vitreous liquefaction, DLS could determine the concurrent aggregation of collagen and other macromolecules that occurs during liquefaction, Raman spectroscopy could identify the presence of specific molecular moieties that provide insight into the pathogenesis, while combined OCT-SLO could image the vitreoretinal interface. Hopefully, the future will witness the combination of these and other techniques into a single noninvasive instrument for research and clinical applications.

References

1 Duke-Elder SW: The nature of the vitreous body. Br J Ophthalmol 1930;14(suppl IV):6.
2 Redslob E: Le corps vitre. Soc Fr Ophtalmol Monogr. Paris, Masson, 1932, pp 174–178.
3 Eisner G: Biomicroscopy of the Peripheral Fundus. New York, Springer, 1973.
4 Worst JGF: Cisternal systems of the fully developed vitreous body in the young adult. Trans Ophthalmol Soc UK 1977;97:550–554.
5 Sebag J, Balazs EA: Morphology and ultrastructure of human vitreous fibers. Invest Ophthalmol Vis Sci 1989;30:1867–1871.
6 Kishi S, Shimizu K: Posterior precortical vitreous pocket. Arch Ophthalmol 1990;108:979–982.
7 Sebag J: Letter to the editor. Arch Ophthalmol 1991; 190:1059.
8 Foulds WS: Is your vitreous really necessary? The role of the vitreous in the eye with particular reference to retinal attachment, detachment and the mode of action of vitreous substitutes. Eye 1987;1:641–664.
9 Sebag J: The Vitreous: Structure, Function and Pathobiology. New York, Springer, 1989.
10 Sebag J: Macromolecular structure of vitreous. Prog Polym Sci 1998;23:415–446.
11 Sebag J, Yee KMP: Vitreous – From biochemistry to clinical relevance; in Tasman W, Jaeger EA (eds): Duane's Foundations of Clinical Ophthalmology. Philadelphia, Lippincott, Williams & Wilkins, 2006, vol 1, chapt 16.
12 Bishop PN: Structural macromolecules and supramolecular organisation of the vitreous gel. Prog Retin Eye Res 2000;19:323–344.
13 Balazs EA: Molecular morphology of the vitreous body; in Smelser GK (ed): The Structure of the Eye. New York, Academic Press, 1961, pp 293–310.
14 Sheehan JK, Atkins EDT, Nieduszynski IA: X-Ray diffraction studies on the connective tissue polysaccharides. Two dimensional packing scheme for threefold hyaluronic chains. J Mol Biol 1975;91:153–163.
15 Balazs EA: Functional anatomy of the vitreus; in Duane TD, Jaeger EA (eds): Biomedical Foundations of Ophthalmology. Philadelphia, Harper & Row, 1984, chapt 17, p 14.
16 Seery CM, Davison PF: Collagens of the bovine vitreous. Invest Ophthalmol Vis Sci 1991;32:1540–1550.
17 Mayne R: The eye; in Royce PM, Steinmann B (eds): Connective Tissue and Its Heritable Disorders: Molecular, Genetic, and Medical Aspects. New York, Wiley-Liss, 2001, pp 131–141.
18 Comper WD, Laurent TC: Physiological functions of connective tissue polysaccharides. Physiol Rev 1978;58:255–315.
19 Scott JE, Chen Y, Brass A: Secondary and tertiary structures involving chondroitin and chondroitin sulphate in solution, investigated by rotary shadowing electron microscopy and computer simulation. Eur J Biochem 1992;209:675–680.
20 Mayne R, Brewton RG, Ren Z-H: Vitreous body and zonular apparatus; in Harding JJ (ed): Biochemistry of the Eye. London, Chapman and Hall, 1997, pp 135–143.
21 Sebag J, Hageman GS: Interfaces. Eur J Ophthalmol 2000;10:1–3.
22 Faulborn J, Bowald S: Microproliferations in proliferative diabetic retinopathy and their relation to the vitreous. Graefes Arch Clin Exp Ophthalmol 1985; 223:130–138.
23 Mann I: The vitreous and suspensory ligament of the lens; in Mann I (ed): The Development of the Human Eye. New York, Grune & Stratton, 1964, p 150.
24 Jack RL: Regression of the hyaloid artery system: an ultrastructural analysis. Am J Ophthalmol 1972;74: 261–272.
25 Balazs EA: Fine structure of the developing vitreous. Int Ophthalmol Clin 1975;15:53–63.
26 Gloor BP: Zur Entwicklung des Glaskörpers und der Zonula. 3. Herkunft, Lebenszeit und Ersatz der Glaskörperzellen beim Kaninchen. Graefes Arch Clin Exp Ophthalmol 1973;187:21–44.
27 Balazs EA, Toth LZ, Ozanics V: Cytological studies on the developing vitreous as related to the hyaloid vessel system. Graefes Arch Clin Exp Ophthalmol 1980;213:71–85.
28 Raymond L, Jacobson B: Isolation and identification of stimulatory and inhibiting growth factors in bovine vitreous. Exp Eye Res 1982;34:267–286.
29 Lutty GA, Mello RJ, Chandler C, et al: Regulation of cell growth by vitreous humour. J Cell Sci 1985;76: 53–65.
30 Jacobson B, Dorfman T, Basu PK, et al: Inhibition of vascular endothelial cell growth and trypsin activity by vitreous. Exp Eye Res 1985;41:581–595.
31 Feeney SA, Simpson DA, Gardiner TA, Boyle C, Jamison P, Stitt AW: Role of vascular endothelial growth factor and placental growth factors during retinal vascular development and hyaloid regression. Invest Ophthalmol Vis Sci 2003;44:839–847.
32 Mitchell CA, Risau W, Drexler HC: Regression of vessels in the tunica vasculosa lentis is initiated by coordinated endothelial apoptosis: a role for vascular endothelial growth factor as a survival factor for endothelium. Dev Dyn 1998;213:322–333.
33 Ito M, Yoshioka M: Regression of the hyaloid vessels and papillary membrane of the mouse. Anat Embryol 1999;200:403–411.

34 McMenamin PG, Djano J, Wealthall R, Griffin BJ: Characterization of the macrophages associated with the tunica vasculosa lentis of the rat eye. Invest Ophthalmol Vis Sci 2002;43:2076–2082.

35 Meeson A, Palmer M, Calfon M, Lang R: A relationship between apoptosis and flow during programmed capillary regression is revealed by vital analysis. Development 1996;122:3929–3938.

36 Dunker S, Glinz J, Faulborn J: Morphologic studies of the peripheral vitreoretinal interface in humans reveal structures implicated in the pathogenesis of retinal tears. Retina 1997;17:124–130.

37 Sebag J, Balazs EA: Human vitreous fibres and vitreoretinal disease. Trans Ophthalmol Soc UK 1985; 104:123–128.

38 Sebag J: Age-related changes in human vitreous structure. Graefes Arch Clin Exp Ophthalmol 1987; 225:89–93.

39 Sebag J: Age-related differences in the human vitreoretinal interface. Arch Ophthalmol 1991;109:966–971.

40 Sebag J: Abnormalities of human vitreous structure in diabetes. Graefes Arch Clin Exp Ophthalmol 1993;231:257–260.

41 Sebag J, Balazs EA: Pathogenesis of cystoid macular edema: an anatomic consideration of vitreoretinal adhesions. Surv Ophthalmol 1984;28(suppl): 493–498.

42 Sebag J: Classifying posterior vitreous detachment – A new way to look at the invisible. Br J Ophthalmol 1997;81:521–522.

43 Schepens CL, Trempe CL, Takahashi M: Atlas of Vitreous Biomicroscopy. Boston, Butterworth Heinemann, 1999.

44 Mainster MA, Timberlake GT, Webb RH, Hughes GW: Scanning laser ophthalmoscopy – Clinical applications. Ophthalmology 1982;89:852–857.

45 Oksala A: Ultrasonic findings in the vitreous body at various ages. Albrecht Von Graefes Arch Klin Exp Ophthalmol 1978;207:275–280.

46 Chu T, Lopez PF, Cano MR, Green RL: Posterior vitreoschisis – An echographic finding in proliferative diabetic retinopathy. Ophthalmology 1996;103: 315–322.

47 Kroll P, Rodrigues E, Hoerle S: Pathogenesis and classification of proliferative diabetic vitreoretinopathy. Ophthalmologica 2007;221:78–94.

48 Green RL, Byrne SF: Diagnostic ophthalmic ultrasound; in Ryan SJ (ed): Retina. St Louis, Mosby, 1989.

49 Sebag J, Buckingham B, Charles MA, Reiser K: Biochemical abnormalities in vitreous of humans with proliferative diabetic retinopathy. Arch Ophthalmol 1992;110:1472–1479.

50 Fujimoto JG, Brezinski ME, Tearney GJ, et al: Optical biopsy and imaging using optical coherence tomography. Nat Med 1995;1:970–972.

51 Srinivasan VJ, Wojtkowski M, Witkin AJ, Duker JS, Ko TH, Carvalho M, Schuman JS, Kowalczyk A, Fujimoto JG: High-definition and 3-dimensional imaging of macular pathologies with high-speed ultrahigh-resolution optical coherence tomography. Ophthalmology 2006;113:2054e1–2054e14.

52 Gupta P, Sadun AA, Sebag J: Multifocal retinal contraction in macular pucker analyzed by combined optical coherence tomography/scanning laser ophthalmoscopy. Retina 2008;28:447–452.

53 Kroll P, Wiegand W, Schmidt J: Vitreopapillary traction in proliferative diabetic vitreoretinopathy. Br J Ophthalmol 1999;83:261–264.

54 Meyer CH, Schmidt JC, Mennel S, Kroll P: Functional and anatomical results of vitreopapillary traction after vitrectomy. Acta Ophthalmol Scand 2007; 85:221–222.

55 Gupta P, Christofferson S, Sadun AA, Sebag J: Quantitative Analysis of Premacular Membranes with Pucker Using Scanning Laser Ophthalmoscope/ Optical Coherence Tomography (SLO-OCT) Imaging. Fort Lauderdale, ARVO, 2007.

56 Sebag J, Rosen RR, Garcia P, et al: Coronal plane imaging with combined OCT-SLO detects macular pucker in macular holes. Meet Club Jules Gonin, Cape Town, 2006.

57 Sebag J, Gupta P, Rosen RR, Garcia P, Sadun AA: Macular holes and macular pucker: The role of vitreoschisis as imaged by optical coherence tomography/scanning laser ophthalmoscopy. Trans Am Ophthalmol Soc 2007;105:121–131.

58 Sebag J: Anomalous PVD – A unifying concept in vitreo-retinal diseases. Graefes Arch Clin Exp Ophthalmol 2004;242:690–698.

59 Sebag J, Ansari RR: Ophthalmic diagnostics. J Biomed Opt 2004;9:8.

60 Sebag J: Diabetic vitreopathy. Ophthalmology 1996; 103:205–206.

61 Aguayo J, Glaser B, Mildvan A, et al: Study of vitreous liquefaction by NMR spectroscopy and imaging. Invest Ophthalmol Vis Sci 1985;26:692–697.

62 Sebag J: Pharmacologic vitreolysis. Retina 1998;18: 1–3.

63 Cheng H, Nair G, Walker TA, Kim MK, Pardue MT, Thulé PM, Olson DE, Duong TQ: Structural and functional MRI reveals multiple retinal layers. Proc Natl Acad Sci USA 2006;103:17525–17530.

64 Zaharchuk G, Busse RF, Rosenthal G, Manley GT, Glenn OA, Dillon WP: Noninvasive oxygen partial pressure measurement of human body fluids in vivo using magnetic resonance imaging. Acta Radiol 2006;13:1016–1024.

65 Ngumah QC, Buchthal SD, Dacheux RF: Longitudinal non-invasive proton NMR spectroscopy measurement of vitreous lactate in a rabbit model of ocular hypertension. Exp Eye Res 2006;83:390–400.
66 Trick GL, Liggett J, Levy J, Adamsons I, Edwards P, Desai U, Tofts PS, Berkowitz BA: Dynamic contrast enhanced MRI in patients with diabetic macular edema: initial results. Exp Eye Res 2005;81:97–102.
67 Nie S, Bergbauer KL, Kuck JFR Jr, Yu NT: Near infrared Fourier transform Raman spectroscopy in human lens research. Exp Eye Res 1990;51:619–623.
68 Sebag J, Nie S, Reiser KA, Charles MA, Yu NT: Raman spectroscopy of human vitreous in proliferative diabetic retinopathy. Invest Ophthalmol Vis Sci 1994;35:2976–2980.
69 Lin SY, Chen KH, Cheng WT, Ho CT, Wang SL: Preliminary identification of Beta-carotene in the vitreous asteroid bodies by micro-Raman spectroscopy and HPLC analysis. Microsc Microanal 2007;13:128–132.
70 Katz A, Kruger EF, Minko G, Liu CH, Rosen RB, Alfano RR: Detection of glutamate in the eye by Raman spectroscopy. J Biomed Opt 2003;8:167–172.
71 Chu B: Laser Light Scattering: Basic Principles and Practice. New York, Academic Press, 1991.
72 Ansari RR: Ocular static and dynamic light scattering: a non-invasive diagnostic tool for eye research and clinical practice. J Biomed Opt 2004;9:46–57.
73 Datiles MB, Ansari RR, Reed GF: A clinical study of the human lens with a dynamic light scattering device. Exp Eye Res 2002;74:93–102.
74 Simpanya MF, Ansari RR, Suh KI, Leverenz VR, Giblin FJ: Aggregation of lens crystallins in an in vivo hyperbaric oxygen guinea pig model of nuclear cataract: dynamic light scattering and HPLC analysis. Invest Ophthalmol Vis Sci 2005;46:4641–4651.
75 Ansari RR, Datiles MB: Use of dynamic light scattering and Scheimpflug imaging for the early detection of cataracts. Diabetes Technol Ther 1999;1: 159–168.
76 Ansari RR, Dunker S, Suh K, Kitaya N, Sebag J: Quantitative molecular characterization of bovine vitreous and lens with non-invasive dynamic light scattering. Exp Eye Res 2001;73:859–866.
77 Sebag J, Ansari RR, Dunker S, Suh SI: Dynamic light scattering of diabetic vitreopathy. Diabetes Technol Ther 1999;1:169–176.
78 Sebag J: Is pharmacologic vitreolysis brewing? Retina 2002;22:1–3.
79 Sebag J: Molecular biology of pharmacologic vitreolysis. Trans Am Ophthalmol Soc 2005;103: 473–494.
80 Sebag J, Ansari RR, Suh KI: Pharmacologic vitreolysis with microplasmin increases vitreous diffusion coefficients. Graefes Arch Clin Exp Ophthalmol 2007;245:576–580.
81 Kroll P: New insights into the diagnosis and treatment of vitreoretinal diseases. Ophthalmologica 2007;221:215.

J. Sebag, MD
7677 Center Avenue
Huntington Beach, CA 92647 (USA)
Tel. +1 714 901 7777, Fax +1 714 901 7770, E-Mail jsebag@VMRinstitute.com